Petrogenesis of Jurassic Granite from the Shuitou Pluton in South Jiangxi Province, South China: Implication for Ion-adsorption REE Enrichment

Shuifeng You , Defu Zhang * , Hanfeng Liu , Meihua Tang , Xinlong Pang , Yufei Wang , Zhiwei Zhang

Posted Date: 28 February 2025

doi: 10.20944/preprints202502.2260.v1

Keywords: Petrogenesis; S-type granite; Ion-adsorption REE deposit; Extensional setting; South China

Article

Petrogenesis of Jurassic Granite from the Shuitou Pluton in South Jiangxi Province, South China: Implication for Ion-adsorption REE Enrichment

Shuifeng You [1], Defu Zhang [1,2,*], Hanfeng Liu [1], Meihua Tang [1], Xinlong Pang [1], Yufei Wang [1] and Zhiwei Zhang [1]

[1] Key Laboratory of Ionic Rare Earth Resources and Environment, Ministry of Natural Resources, Jiangxi College of Applied Technology, Ganzhou 341000, China

[2] School of Earth Science, East China University of Technology Nanchang 330013, China

* Correspondence: zhangdefu@jxyy.edu.cn

Abstract: Ion-adsorption rare earth deposits are mainly formed by the weathering and leaching of the granite ore-forming parent rocks, and the heavy rare earth resources in the world dominantly occur within this type of deposits. In this study, we take the Shuitou pluton, the Late Jurassic rare earth element (REE) ore-forming parent rocks, as the research object, and elucidate the REE enrichment process in the granites through the chronology, rock geochemistry and isotope geochemistry analyses. The results show that the zircon U–Pb age of the Shuitou pluton is ~150 Ma, and the monazite U–Pb age is ~145 Ma, both indicating the pluton was formed in the Yanshan Stage. The rocks have high content values of SiO_2 (72.85–75.55 wt%), Al_2O_3 (12.85–14.63 wt%), and K_2O (4.46–5.27 wt%), with the A/CNK values of 1.05–1.19, the differentiation index (DI) values of 87.48–95.59, the zircon saturation temperature values of 689–746 ℃, the Nb/Ta ratios of 2.72–9.54, and the Zr/Hf ratios of 7.12–26.11; besides, the rocks also contain peraluminous minerals muscovite and garnet. All these indicate that rocks belong to highly fractionated S-type granite. The $\varepsilon_{Hf}(t)$ values of zircon and monazite range from –10.04 to –6.78 and –9.3 to –8.2, respectively, indicating that the magma mainly originated from the Proterozoic crustal metamorphic sedimentary rocks. In the extensional tectonic setting of South China, high temperature promotes the melting of the REE-enriched accessory minerals, and the higher content value of F increases the solubility of the REEs in the molten mass. The presence of the heavy rare earth minerals such as garnet in the rocks makes the rocks have a high heavy rare earth element (HREE) content, and the REE-enriched minerals such as titanite, bastnäsite, and allanite provide the material conditions for the formation of the ion-adsorption REE deposits.

Keywords: petrogenesis; S-type granite; ion-adsorption REE deposit; extensional setting; South China

1. Introduction

The 17 rare earth elements, including lanthanide series elements and transition metal elements Sc and Y, have been widely applied in new energy, semiconductor materials, military, medicine and other high-tech fields because of their unique atomic structures and excellent photoelectromagnetic properties, and have been listed as a key or stategic resource type by many countries [1]. The ion-absorption type rare earth element (REE) deposits in China are mainly distributed in South China, such as the Longnan deposit in Jiangxi Province and the Guposhan deposit in Guangxi Province. Up to now, more than 170 ion-adsorption REE deposits have been found in China, providing 35% of global rare earth resources and about 90% of global heavy rare earth resources [2]. The ion-adsorption rare earth deposits are formed by the weathering and leaching of the REE-enriched rocks such as granite, volcanic rock, metamorphic rock, basaltic rock and carbonate rock, among which granite is

 doi:10.20944/preprints202502.2260.v1

the most important ore-forming parent rock and the only parent rock type that can form heavy rare earth deposits [5]. In the weathering process of the ore-forming parent rocks of the ion-adsorption rare earth deposit, the REE-enriched minerals such as allanite, bastnaesite, and apatite broke and decomposed, and released the rare earth elements which infiltrated downward with rain water and migrated constantly toward the lower part of the weathering crust. As the result, the the rare earth elements were adsorbed in the form of ion adsorption phase on the clay minerals such as kaolinite and halloysite, and eventually enriched and mineralized in the lower part of the fully weathered layer and the upper part of the semi-weathered layer [6] .

Studies have shown that the rare earth elements are influenced by the factors such as microbial activities, the adsorption/desorption of the elements on/from the iron manganese oxides and clay minerals, and the complexation of the elements with CO_3^{2-} /HCO_3^- during the migration, differentiation and enrichment of these elements in the weathering crust [7,9]. However, the pre-enrichment of the rare earth elements in granite plays a decisive role in the formation of ion-adsorption rare earth deposits. In the weathering crust, the REE assemblage pattern largely inherits the REE assemblage pattern of the parent rocks. Specifically, the parent rocks enriched with light rare earth elements form light rare earth deposits, while the parent rocks enriched with heavy rare earth elements form heavy rare earth deposits [6,10,11]. There are different viewpoints on the pre-enrichment mechanism of the rare earth elements in granite nowadays. Previous studies showed that the pre-enrichment of the REEs in granite is mainly related to magma-hydrothermal activities [11], but some others believe that it is related to the magmatic source region or to the replacement of HREE-enriched mantle-derived fluids [19,20]. The ion-adsorption rare earth ore-forming granites in South China are mostly formed in the Mesozoic strata. The geochemistry shows that the ore-forming granites are peraluminous, high-potassium calc-alkaline granites with higher I_{sr} values and lower $\varepsilon_{Nd}(t)$ values, formed by the strong differentiation evolution of the magma derived from the high maturity crust [21]. The diagenetic age values are especially concentrated in 150–190 Ma with the back-arc extensional tectonic setting caused by the Paleo-Pacific Plate subductions [22,23]. The ion-adsorption rare earth deposits formed during this period are numerous and have richest types [24] . But the relationship between the extensional tectonic setting and the enrichment of the rare earth elements in South China is still unclear. Therefore, the detailed geochemical studies on the parent rocks of the ion-adsorption rare earth deposits are helpful to reveal the influence of the source region properties of the parent rocks and the magmatism on the rare earth mineralization, and the relationship between these factors and the Mesozoic extensional tectonics setting in South China.

Mesozoic granites associated with the ion-adsorption rare earth mineralization are widely distributed in southern Jiangxi Province. The Shuitou pluton, as one of the ion-adsorption rare earth ore-forming plutons, has been traditionally believed being formed during the Caledonian period, but relevant supporting data such as the chronological data are still lacking. In this study, the Shuitou pluton was analyzed from the aspects of the lithography, zircon and monazite U–Pb geochronology, and zircon Lu–Hf and monazite Nd isotopology; the magmatic source region and the magmatic evolution process were clarified, and the Mesozoic tectonic-magma-rare earth mineralization model has been established.

2. Geological Background and Petrology

2.1. Geological Background

The South China Plate was formed by splicing of the Cathaysia Block and the Yangtze Block along the Jiangshan-Shaoxing Fault in the Neoproterozoic era (Figure 1, [25]), and had undergone three tectonothermal events in Paleozoic, Early Mesozoic and Late Mesozoic respectively, forming large-scale magmatic rocks, and rare metal and non-ferrous metal deposits [26] . Mesozoic granites and contemporaneous volcanic rocks are widely distributed in the South China Plate. With the subduction of the Jurassic Paleo-Pacific Plate to the southwest flat slab, the subsequent breaking of the slab, and the continuous increase of the subduction angle, a large number of Jurassic-Cretaceous

 doi:10.20944/preprints202502.2260.v1

magmatic rocks become gradually younger toward the southeast coast [22,23],[27,29]. The Southern Jiangxi Region lies within the Cathaysia Block in the eastern South China Plate, with Jiangshan-Shaoxing Fault Zone in the northwest and the Zhenghe-Dapu Fault Zone in the southeast of the Cathaysia Block. Magmatic rocks are well developed in various geological periods, with the Yanshanian granites occupying the largest area, accounting for 70% of the whole Southern Jiangxi Region (Fg.2a). A set of Precambrian crystalline basement develops in this region, overlain by the the Sinian-Cambrian sedimentary cover, and the Devonian, Carboniferous and Cretaceous Series are in angular unconformity contact with the underlying Cambrian Series.

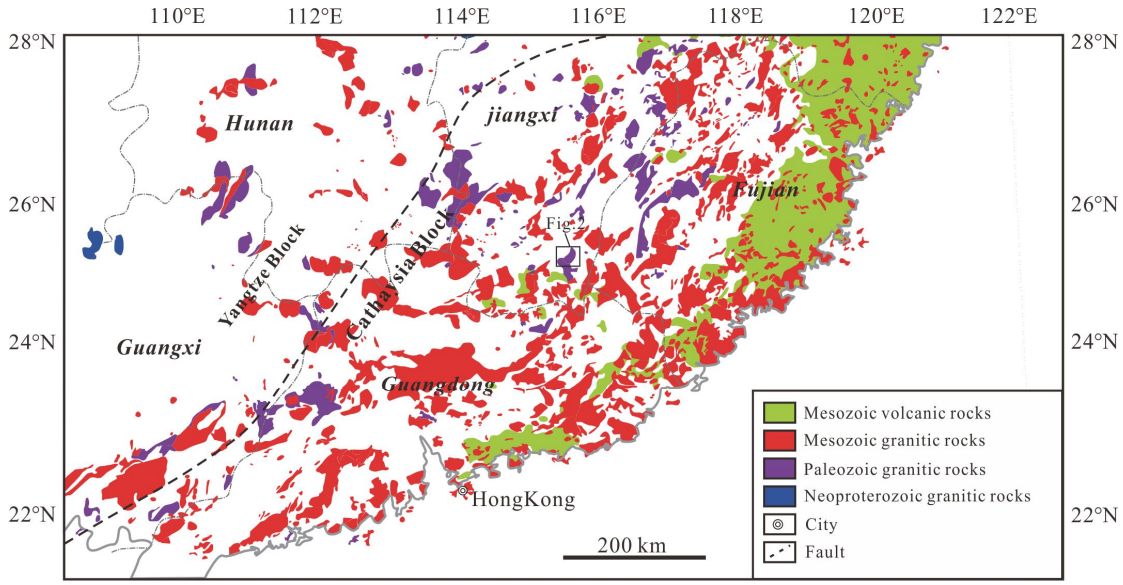

Figure 1. Distribution of granites and volcanic rocks in South China (after Li et al., 2019[30]).

The Shuitou pluton is located at the junction of the Youshui Town in Huichang County and the Tianxin Town in Anyuan County, Ganzhou City. The main pluton body lies in the Huichang County, with the exposed area of about 70 km^2. Recent study results of the author's team show that the granites in the study area are mainly composed of the Shitouping plutons of the Yanshanian Stage, and the Chengkeng and Sunwu plutons of the Caledonian Stage (Figure 2b), rather than the Caledonian Shuitou and Sanbiao plutons as previously thought [17]31,[32]. The diagenetic ages of the Shitouping, the Chengkeng and the Sunwu plutons are ~140 Ma [18] , ~450 Ma and ~450 Ma [32] respectively. As the oldest exposed strata in the region, the Neoproterozoic Taoxi Formation mainly exposes on both sides of the near north-south trending Huichang Basin. The exposed Nanhuan to Cambrian systems are relatively continuous, with the lithology being the medium to thick layered, shallow metamorphic greywacke interbedded with thin-layered slate and a small amount of silicolite. The Jurassic system is mainly exposed in the northern part of the study area as a set of miscellaneous, terrigenous clastic rock. The early Cretaceous strata is a set of neutral to acid volcanoclastic rock and lava, mainly occurring along the phacolith and in the Caifang volcanic basin, with the forming age being the early period of the Early Cretaceous epoch [33,34]. The distribution of the Late Cretaceous volcanic rock are obviously controlled by the regional NNE-trending fault zones (Figure 2b).

 doi:10.20944/preprints202502.2260.v1

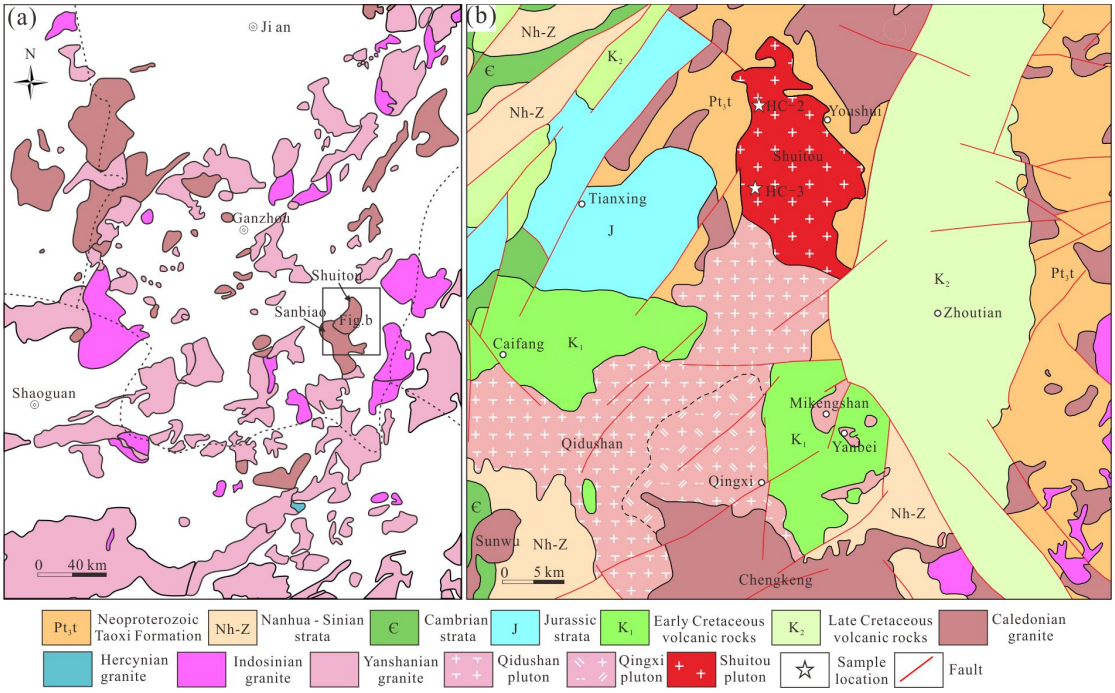

Figure 2. (a) Distribution of granites in Southern Jiangxi Region (after Sun et al., 2006[35]), and (b) Simplified geological map of Shuitou pluton.

2.2. Petrology

The coarse-grained biotite syenogranite (CGBG) sample (ST-5) is flesh-red in color (Figure 3a) with a granitic texture and a blocky structure, and mainly composed of plagioclase, potassium feldspar, quartz, and a small amount of biotite. The plagioclase is in the hypidiomorphic tabular shape, with polysynthetic twins well developed (Figure 3b); some plagioclase (32 vol%) develops annular structures and is clayified within the annular structures (Figure 3c, d). The surface of potassium feldspar (28 vol%) experiences weak clayification (Figure 3e). The quartz (35 vol%) is heteromorphic granular in shape, with a small apart having wavy extinction (Figure 3b). The biotite (5 vol%) has undergone complete chloritization on the whole, and only retains its flake shape (Figure 3f); a large amount of mafic components exsolve along the cleavage cracks and the edges, and form some opaque metallic minerals.

The fine-grained two-mica monzogranite (FTMG) sample (ST-12) is gray in color (Figure 3g), with a granitic texture and a blocky structure, and mainly composed of plagioclase, potassium feldspar, quartz, and a small amount of biotite and muscovite. The plagioclase (29 vol%) is in the hypidiomorphic tabular shape, with polysynthetic twins well developed (Figure 3h). The potassium feldspar (34 vol%) is in the heteromorphic tabular shape, mainly composed of perthite with striped structures well developed and clayification occurring on the surface (Figure 3i, j). The quartz (30 vol%) is heteromorphic granular in shape, with a small part having wavy extinction (Figure 3h). The biotite (3 vol%) is in the hypidiomorphic-heteromorphic flaky shape (Figure 3k), and has obvious pleochroism; some mafic components exsolve along the cleavage cracks and the edges and form opaque metallic minerals. The muscovite (4 vol%) is heteromorphic flaky in shape and has bright interference colors (Figure 3l).

 doi:10.20944/preprints202502.2260.v1

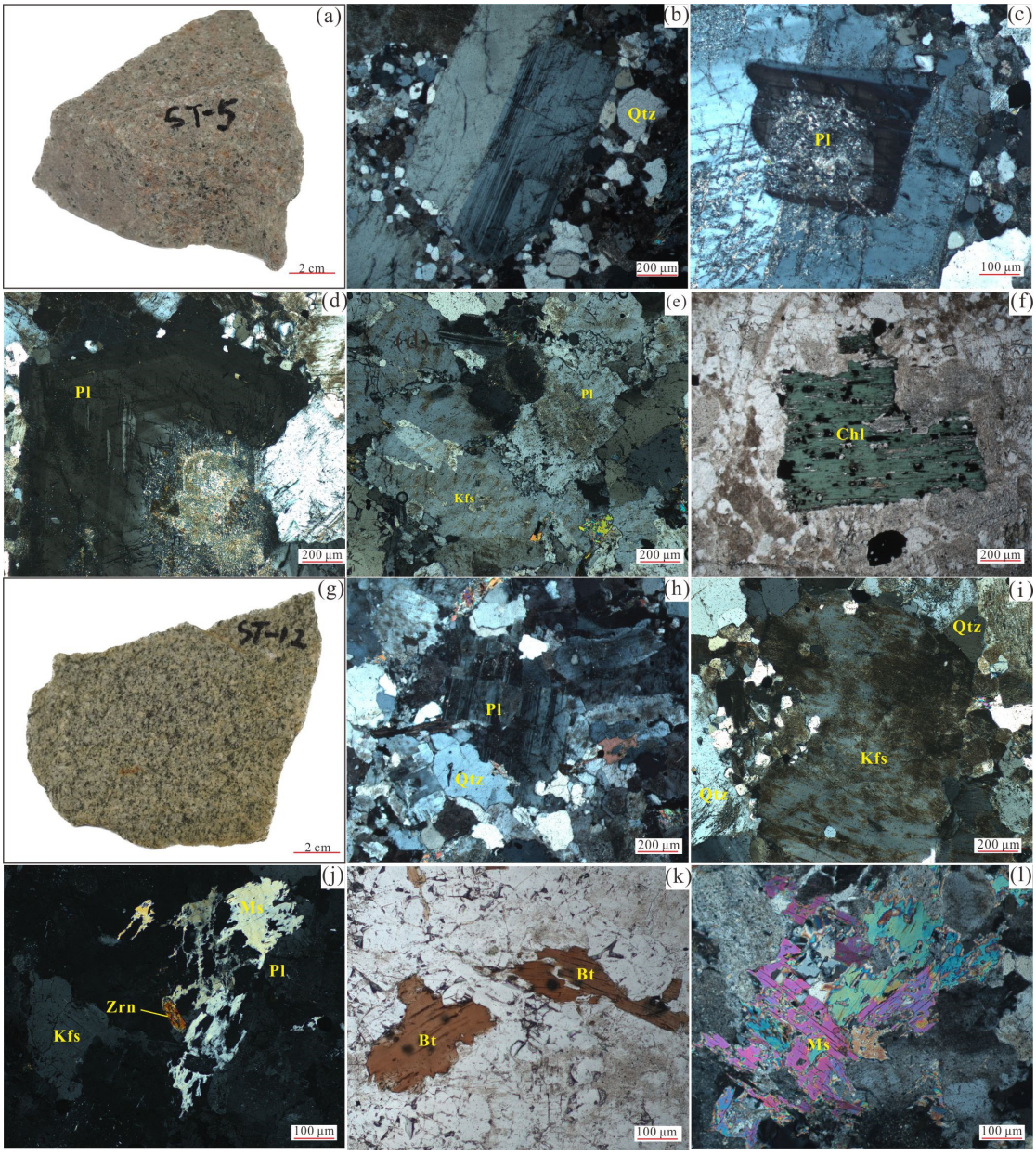

Figure 3. Hand specimens and microscopic microphotographs of the Shuitou Pluton. Bt–Biotite; Chl–Chlorite; Kfs–Potassic feldspar; Ms–Muscovite; Pl–Plagioclase; Qtz–Quartz; Zrn–Zircon.

The rare earth minerals contained in the bedrock include apatite, allanite, titanite, bastnaesite, xenotime, monazite, zircon and garnet, etc. (Figure 4a-f), whereas the rare earth minerals derived from the magma crystallization include apatite, zircon, and thorite, etc. (Figure 4a, e). The apatite and allanite are altered to xenotime and monazite respectively by hydrothermal action (Figure 4a, b); the pores in the allanite produced by the metasomatism of the hydrothermal fluids are filled by the bastnaesite (Figure 4c-e); the titanite and allanite co-grow (Figure 4e), and the garnet fills in the feldspar (Figure 4f).

 doi:10.20944/preprints202502.2260.v1

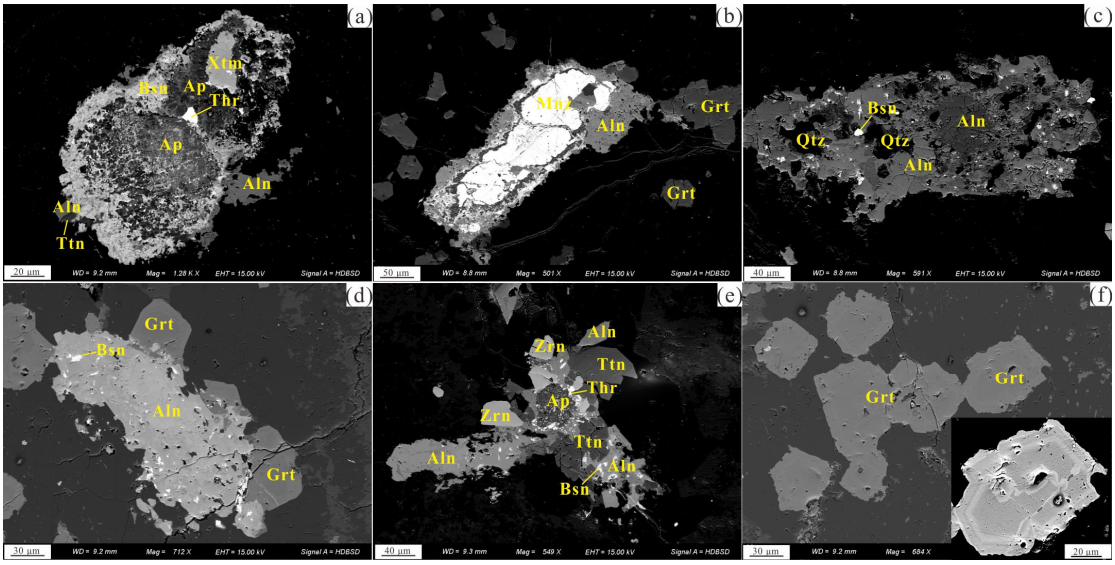

Figure 4. Back-scattered electron (BSE) images of REE-enriched accessory minerals in Shuitou pluton. Aln–Allanite; Ap–Apatite; Bsn–Bastnäsite; Thr–Thorite; Ttn–Titanite; Mnz–Monazite; Qtz–Quartz; Grt–Garnet; Zrn–Zircon.

3. Analytical Methods

3.1. Zircon and Monazite U–Pb Dating

The zircon and monazite selection from the coarse-grained biotite syenogranite (CGBG) sample (HC-2) and the fine-grained two-mica monzogranite (FGTG) sample (HC-3), target making and photography are carried out and finished by Langfang City Chenchang Rock and Mineral Testing Technology Service Co., Ltd. The U–Pb dating of zircon and monazite is completed by the State Key Laboratory of Nuclear Resources and Environment, East China University of Science and Technology. The Agilent 7900 ICP–MS is applied to connect the GeoLasHD laser ablation system, and the laser ablation spot diameters used for zircon and monazite are 32μm and 16μm, respectively. Zircon U–Pb dating uses the standard zircon 91500 as the external standard, and one standard sample is analyzed after every five samples have been analyzed, with the NIST610 glass being used as standard to calibrate the trace element values in zircon samples. Monazite U–Pb dating uses the standard monazite 44069 as the external standard, and also one standard sample is analyzed after every 5 samples have been analyzed, with the NIST610 glass is used as standard to calibrate the trace element values in monazite samples. The ICPMSDataCal program is used to conduct the offline processing of the analytical data [36]. The harmonic curve age and weighted average age of zircon and monazite are calculated by using Isoplot/Exver 3 [37].

3.2. Zircon Hf and Monazite Nd In-Situ Analyses

The in situ Lu–Hf isotope analyzing and testing of the zircon U–Pb age valid points are performed by means of the Nu Plasma MC-ICP-MS and the accompanying RESONICS S-155 excimer ArF laser ablation system. This work is finished by the Nanjing Hongchuang Geological Exploration Technology Service Co., Ltd. The energy density of the deep ultraviolet beams emitting by the excimer laser generator is 3.5 J/cm^2, the laser ablation spot diameter used is 50 μm, and the frequency used is 9 Hz. One standard zircon sample is tested every five zircon sample tests. The $\varepsilon_{Hf}(t)$ value is calculated by using the ratios of the chondrite $^{176}Lu/^{177}Hf$ and $^{176}Hf/^{177}Hf$ reported by Blichert-Toft et al. (1997)[38]. The present values of the depleted mantle' $^{176}Lu/^{177}Hf$ and $^{176}Hf/^{177}Hf$ reported by Griffin et al. (2000)[39] and the average value of the crust' $(^{176}Lu/^{177}Hf)_{CRUST}$ ratio 0.015[40] are used to calculate the Hf two-stage model age.

 doi:10.20944/preprints202502.2260.v1

The in situ testing of Nd isotope of monazite is performed by using the LA–MC–ICP–MS (RESOlution SE 193nm + Neptune plus) at Kehui Testing (Tianjin) Technology Co., Ltd. The laser ablation spot diameter used is 20 μm, the frequency is 6 Hz, and the energy density is 5 J/cm^2. One standard monazite sample is tested after every five monazite samples have been tested. All Nd isotope data are processed by the Iso-Compass software [41]. Refer to Xu et al., 2015[42] for detailed analysis and test methods.

3.3. Whole-Rock Major and Trace Element Analyses

The fresh sample is ground to less than 200 mesh for test and analysis. The whole rock major and trace element analysis is completed in Aoshi Analysis and Testing (Guangzhou) Co., Ltd. The main element analysis is conducted by using the X-ray fluorescence spectrometer (XRF), with the instrument being PANalytical PW2424, which has the relative deviation of less than 5% (RD < 5%). The trace elements analysis is conducted by using the inductively coupled plasma mass spectrometer (ICP–MS), with the instrument being Agilent 7900, which has the relative deviation of less than 10% (RD < 10%). The standard samples used are GSR3 and GSR5.

4. Aanalysis Results

4.1. Zircon U–Pb Dating

The zircon U–Pb isotopic age data of the coarse-grained biotite syenogranite (CGBG) (HC-2) and the fine-grained two-mica monzogranite (FTMG) (HC-3) samples from the Shuitou pluton are listed in Supplementary Table S1. Zircon samples are dominantly colorless or light yellow, and hypiodiomorphic columnar in shape. The length of these samples ranges from 80 to 220 μm, with the aspect ratios being 1:1–3:1, indicating unique oscillatory zoning pattern of the magmatic zircon (Figure 5a, c). The content values of thorium and uranium are 60–598 ppm and 99–1549 ppm respectively in the coarse-grained biotite syenogranite (HC-2) samples, with the Th/U ratios being 0.30–0.90 (Figure 5f), the positive δCe anomaly, and the enrichment of the heavy rare earth elements (Figure 5e), showing the characteristics of magmatic zircon. The concordia degree of the 25 test points is greater than 90%, with the test points being clustered on or near the concordia line (Figure 5a). The zircon $^{206}Pb/^{238}U$ age values are 146–165 Ma, with the weighted average age of (151.2 ± 1.70) Ma (MSWD = 1.08, n = 25) (Figure 5b), representing the formation age of the rock. The content values of thorium and uranium are 64–302 ppm and 111–923 ppm respectively in the fine-grained two-mica monzogranite (HC-3) samples, with the Th/U ratios being 0.28–0.76 (Figure 5f), similar to the geochemical characteristics of the coarse-grained biotite syenogranite samples (Figure 5e), also indicating the magmatic zircon. The concordia degree of the 20 test points is greater than 90%, with all test points being clustered on or near the concordia line (Figure 5c). The zircon $^{206}Pb/^{238}U$ age values are 146–154 Ma, with the weighted average age of (150.1 ± 2.90) Ma (MSWD = 0.09, n = 20) (Figure 5d), representing the formation age of the rock.

Preprints.org (www.preprints.org) | NOT PEER-REVIEWED | Posted: 28 February 2025 doi:10.20944/preprints202502.2260.v1

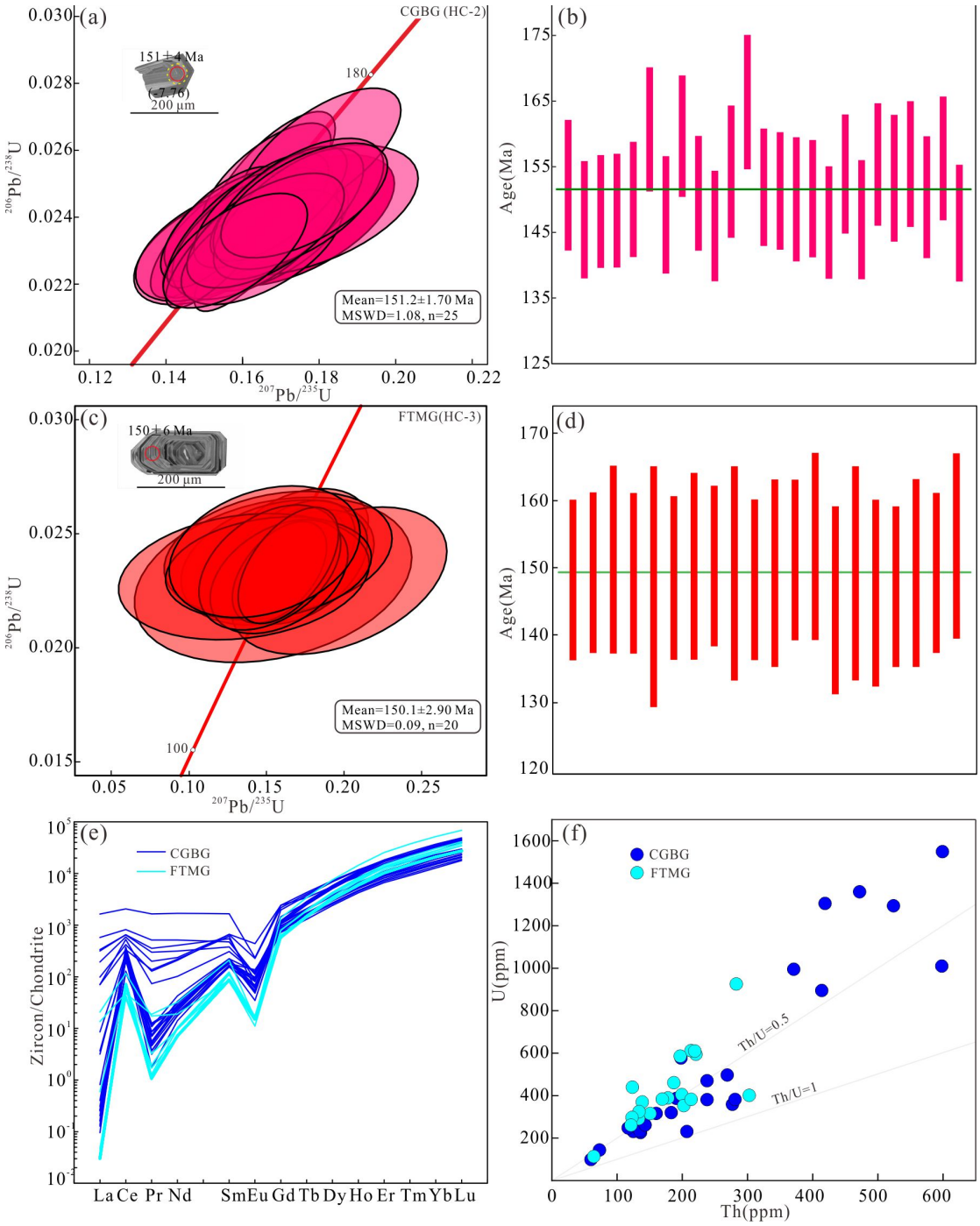

Figure 5. (a-d) Zircons U–Pb concordia diagram and weighted average age, (e) Zircons chondrite-normalized REE pattern, (f) Th vs. U diagram for the Shuitou pluton. The red circle is for U–Pb dating and the yellow circle is for Hf isotopic analysis.

4.2. Monazite U–Pb Dating

The monazite U–Pb isotopic data of the fine-grained two-mica monzogranite (FGTG) sample from the Shuitou pluton are listed in Supplementary Table S2. The monazite samples are dominantly in irregular shape, with the length ranging from 50 to 120 μm and the aspect ratios being 1:1–3:1. Most monazite samples are dark gray and have cracks, with obvious marks of melt alteration; a small part of monazite samples have striped structures with alternating light and dark colors (Figure 6a), which may be caused by the uneven contents of the U, Th and Pb in their growth process. The content values of thorium and uranium are 63417–264274 ppm and 5836–14384 ppm respectively in the monazite samples, with the Th/U ratios being 7.32–25.81. Among the 22 test points, the age value of

 doi:10.20944/preprints202502.2260.v1

point 7 is too small and that of point 8 is too large, therefore, both values are dropped off. The remaining 20 test points are all clustered on or near the concordia line (Figure 6a), with the weighted average age of (145.3 ± 1.40) Ma (MSWD = 0.58, n = 20) (Figure 6b), representing the formation age of the rock.

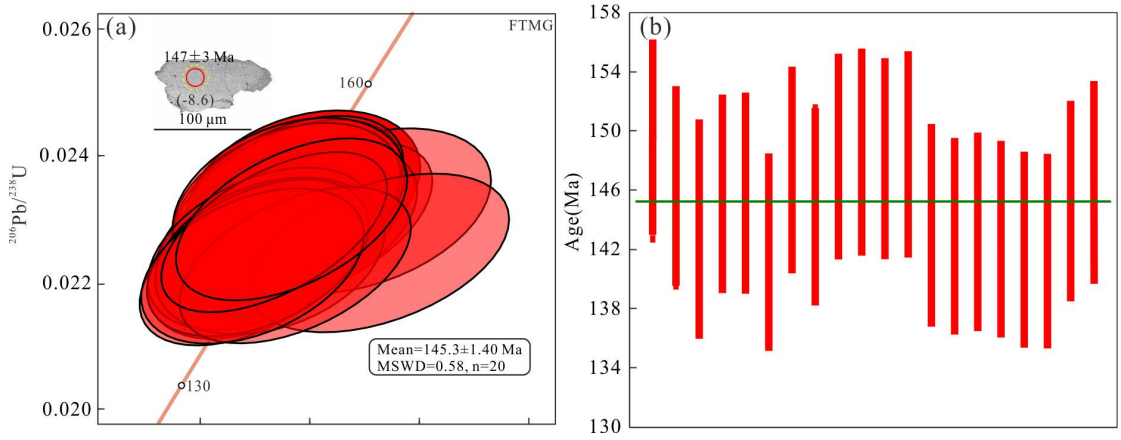

Figure 6. (a) Monazite U–Pb concordia diagram, and (b) Weighted average age of the Shuitou pluton. The red circle is for U–Pb dating and the yellow circle is for Nd isotopic analysis.

4.3. Whole-Rock Geochemical Characteristics

4.3.1. Major Elements

The whole-rock major and trace element data of the coarse-grained biotite syenogranite (CGBG) and the fine-grained two-mica monzogranite (FGTG) samples from the Shuitou pluton are listed in Supplementary Table S3, showing the similar geochemical characteristics of the CGBG and the FTMG. The content values of SiO_2, Al_2O_3, K_2O, Na_2O and the total alkali (K_2O+Na_2O) are 72.85–75.55 wt%, 12.85–14.63 wt%, 4.46–5.27 wt%, 2.72–4.50 wt% and 7.99–9.04 wt%, respectively (Figure 7a, b). The ratios of K_2O/Na_2O are 1.01–1.94 (avg. 1.43), and the differentiation index (DI) values are 87.48–95.59 (avg. 92.87). Comparatively, the content values of the FeOt, MgO and CaO are higher in the CGBG (Figure 8). The sample points are projected into the sub-alkaline granite region in the SiO_2 vs. (K_2O+Na_2O) diagram (Figure 7a), whereas the sample points falls into the high-potassium calc-alkaline series to shoshonite series region (Figure 7b). The aluminum saturation index (A/CNK) values are 1.05–1.19, all samples falling into the peraluminous region in the A/CNK vs. A/NK diagram (Figure 7c). In the SiO_2 vs. FeOt/(FeOt+MgO) diagram, all samples show ferroan characteristics (Figure 7d).

 doi:10.20944/preprints202502.2260.v1

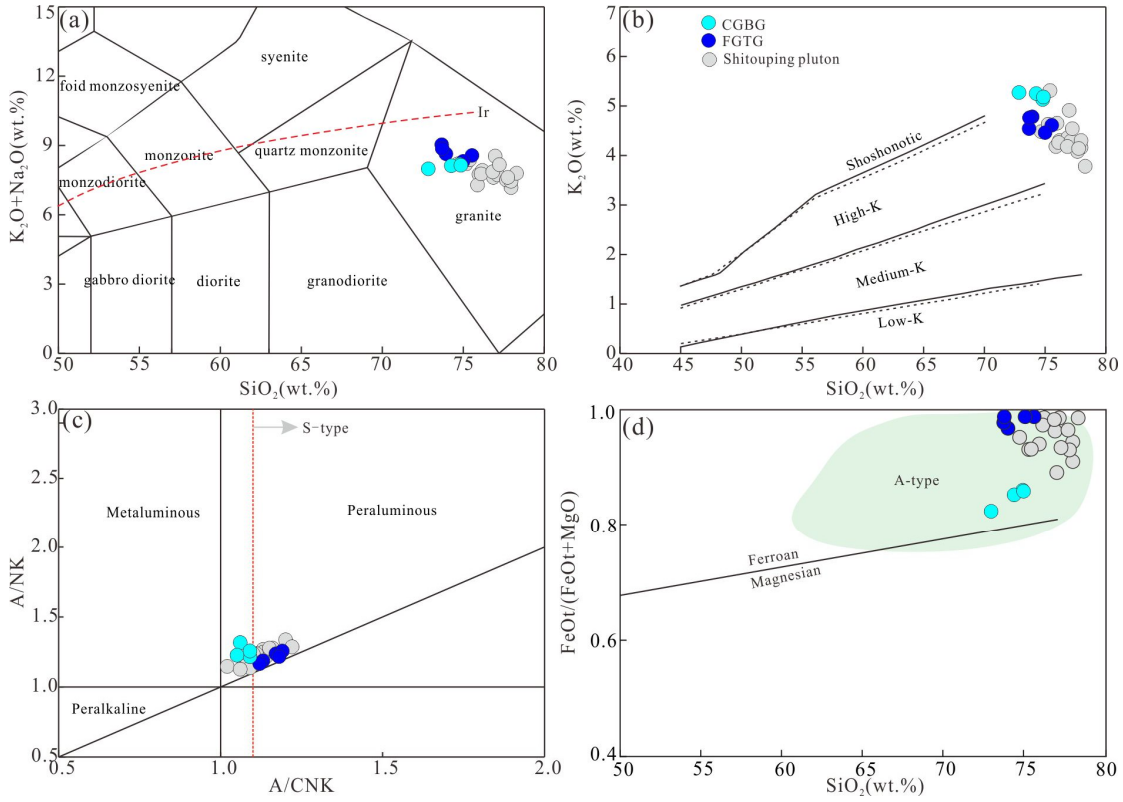

Figure 7. (a) SiO_2 vs. (K_2O+Na_2O) (Middlemost, 1994[43]), (b) SiO_2 vs. K_2O (solid line after Peccerillo and Taylor, 1976[44]; dotted line after Middlemost, 1985[45]), (c) A/CNK vs. A/NK (Maniar et al., 1989[46]) and (d) SiO_2 vs. FeOt/(FeOt+MgO) (Frost et al., 2001[47]) diagrams for the Shuitou pluton. Data for Shitouping pluton are from references [18,32].

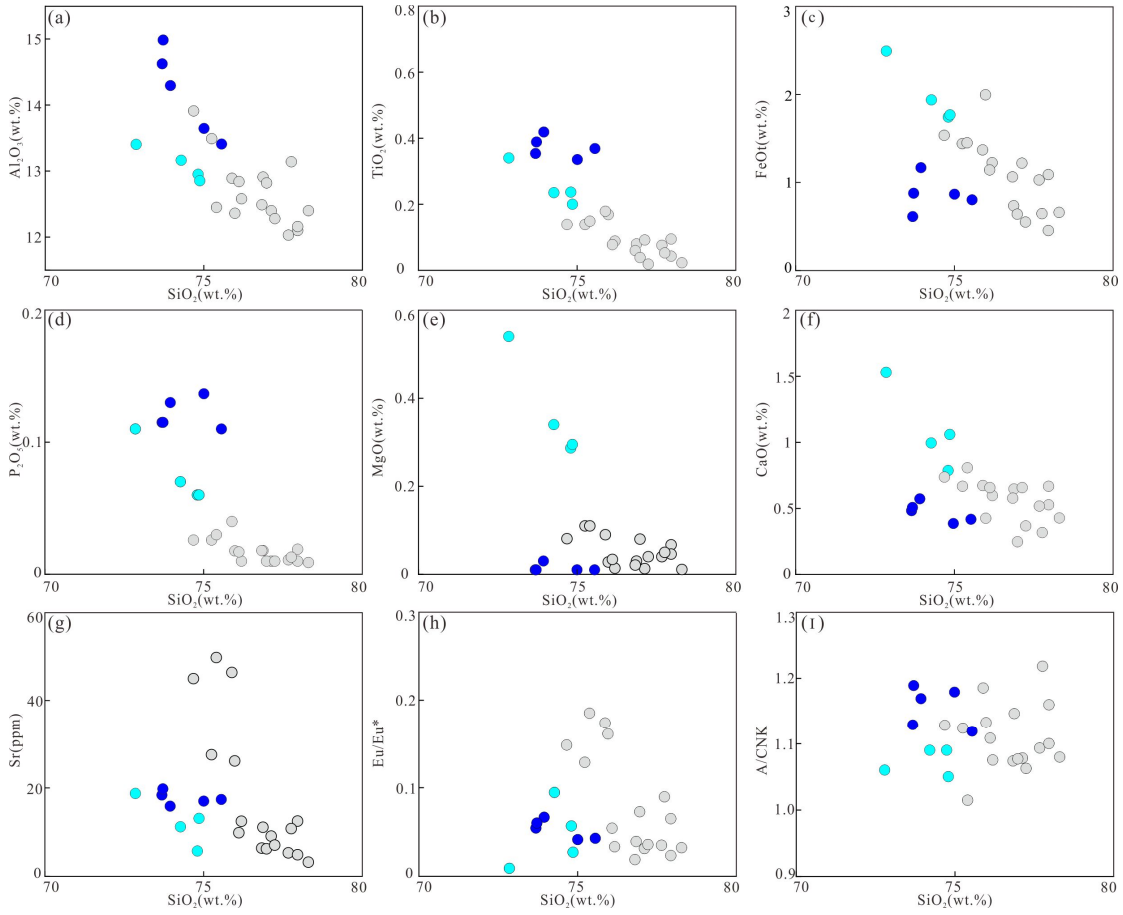

 doi:10.20944/preprints202502.2260.v1

Figure 8. Harker diagram for Shuitou pluton. The data sources are same as Figure 7.

4.3.2. REE and Trace Elements

The total amount of the rare earth elements in the coarse-grained biotite syenogranite (CGBG) and the fine-grained two-mica monzogranite (FGTG) samples from the Shuitou pluton is 166–236 ppm. The chondrite-normalized rare earth element curves show that the heavy rare earth elements (HREEs) are relatively more enriched than the light rare earth elements (LREEs), with $(La/Yb)_N$ = 0.22–0.83 and obvious negative Eu anomalies (Eu/Eu* = 0.03–0.09), indicating that the separation and crystallization of plagioclase and potassium feldspar are comparatively strong during the magma crystallization process (Figure 9a). The primitive mantle-normalized trace element diagram shows that the elements such as Rb, Th, U, and Nd are relatively enriched, whereas the elements such as Ba, Nb, Sr, P, and Ti are relatively depleted (Figure 9b). The values of Sr and Yb are 5.63–19.70 and 6.77–23.45 ppm, respectively, indicating the low Sr- and high Yb- type granite, and suggesting the Shuitou pluton was formed in the crustal thinning tectonic setting with low pressure (< 0.8 Gpa) and shallow depth (< 30km)[48].

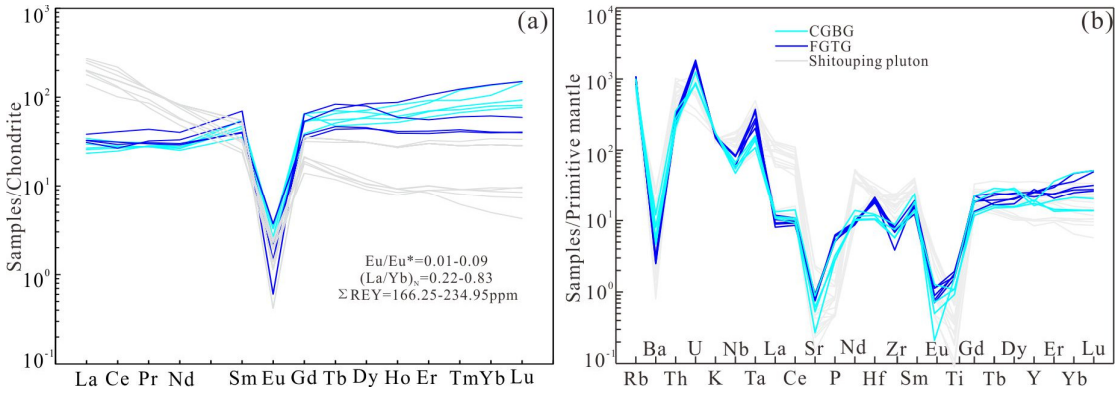

Figure 9. (a) Chondrite-normalized REE patterns (normalized values from Sun and McDonough, 1989[49]), and (b) Primitive mantle-normalized trace element (normalized values from Sun and McDonough, 1989[49]) spider diagrams for the Shuitou pluton. The data sources are same as Figure 7.

4.4. Zircon Hf Isotopic Results

The zircon Hf isotope data of the coarse-grained biotite syenogranite (CGBG) samples from the Shuitou pluton are shown in Supplementary Table S4. The relatively high closure temperature of the zircon Lu–Hf isotopic system [47] provides important constraints on the genetic evolution of zircon. The ratios of the zircon $^{176}Yb/^{177}Hf$ and $^{176}Lu/1^{77}Hf$ are 0.022590–0.044477 and 0.000740–0.001446 respectively, and the $^{176}Lu/^{177}Hf$ ratios are all less than 0.02, indicating a low accumulation of the radioactive Hf element. Therefore, the initial $^{176}Hf/^{177}Hf$ ratio can represent the $^{176}Hf/^{177}Hf$ ratio at the time when zircon formed [50]. The zircon $f_{Lu/Hf}$ values range from –0.96 to –0.98, significantly lower than the $f_{Lu/Hf}$ value (–0.34) of the ferromagnesian crust [51] and the $f_{Lu/Hf}$ value (–0.72) of the salic crust [52]. Therefore, the two-stage model age can represent the time when the source region materials were extracted from the depleted mantle.

The zircon $^{176}Hf/^{177}Hf$ ratios are 0.282401–0.282488, with the relatively uniform Hf isotope compositions and a weighted average value of 0.282442; the corresponding $\varepsilon_{Hf(t)}$ values are –10.04 to –6.78, with an average value of –8.50 (Figure 10a). The two-stage model age values range from 1633 to 1832 Ma, with an average of 1738 Ma (Figure 10b).

 doi:10.20944/preprints202502.2260.v1

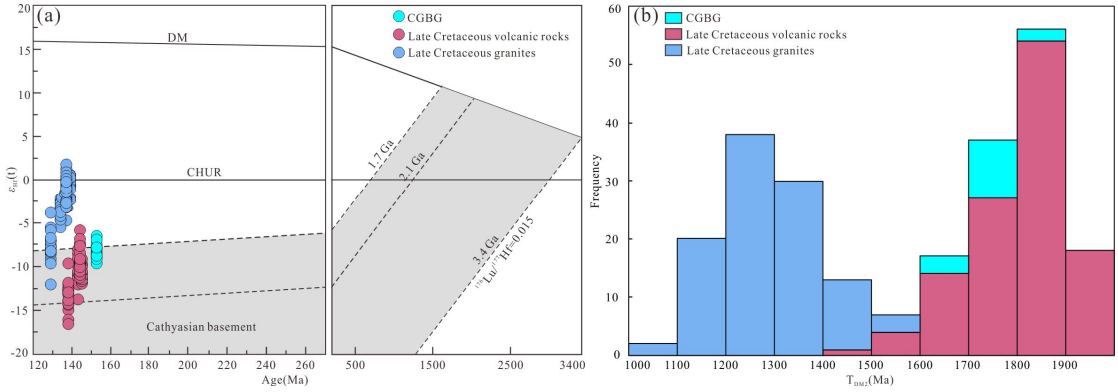

Figure 10. (a) Zircons age vs. $\varepsilon_{Hf}(t)$ diagram, and (b) T_{DM2} frequency distribution histogram for CGBG. The data of late Cretaceous volcanic rocks and granites are from references [32].

4.5. Monazite Nd Isotopic Results

The monazite Nd isotope data of the fine-grained two-mica monzogranite (FGTG) samples from the Shuitou pluton are shown in Supplementary Table S5. The monazite $^{143}Nd/^{144}Nd$ ratios range from 0.512096 ± 0.000016 to 0.512143 ± 0.00018; the corresponding $\varepsilon_{Nd}(t)$ values are –9.3 to –8.2, with an average value of –8.6, and the two-stage model age values range from 1684 to 1613 Ma, with an average value of 1645 Ma (Figure 11).

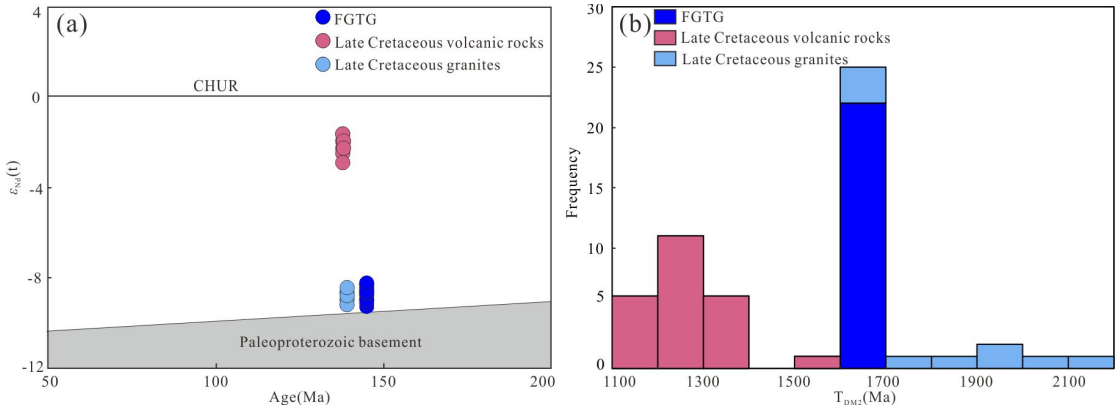

Figure 11. (a) Monazite age vs. $\varepsilon_{Nd}(t)$ diagram, and (b) T_{DM2} frequency distribution histogram for CGBG. The data of late Cretaceous volcanic rocks and granites are from references [18,53].

5. Discussion

5.1. Petrogenesis of Shuitou Pluton

Granites can be classified into I-, S-, A- and M-types based on their genetic types [54]. M-type granite is formed by the separation and crystallization of the mantle-derived basic magma, and is rarely found in nature [55]. I-type granite is mainly found to be igneous rock in its source region, with hornblende as the diagnostic mineral, and the Sr, Nd, and Hf isotopes being relatively depleted. Besides, the aluminum saturation index (A/CNK < 1.1) and FeOt content are low, and the content values of SiO_2 and P_2O_5 are in negative correlation [55,56]. S-type granite is mainly metasedimentary rock in its source region with the primary garnet, muscovite and iolite as diagnostic minerals. The aluminum saturation index A/CNK is greater than 1.1, and the content value of P_2O_5 is greater than 0.2 wt%[56,57]. A-type granite formed at relatively high temperature [58,59], is characterized by the non-orogenic, alkaline and relatively water-poor environment in its source region [60], with the mineral combinations mainly including quartz, dark ferromagnesian minerals and alkaline feldspar.

 doi:10.20944/preprints202502.2260.v1

The values of Zr+Nb+Ce+Y > 350 ppm and 10000Ga/Al > 2.6 are taken as the discriminant indicators of A-type granite.

The samples from Shuitou pluton have relatively low 10000Ga/Al values (2.56–3.01), and most values fall into I-type region or S-type region in the (Zr+Nb+Ce+Y) vs. 10000Ga/Al and the (Zr+Nb+Ce+Y) vs. (K_2O+Na_2O)/CaO diagrams (Figure 12a, b). The whole rock zircon saturation temperatures are 689–746 ℃ (avg. 729 ℃) (Figure 13b), significantly different from the formation temperature of A-type granite, which is greater than 800 ℃ [61]. The Shuitou pluton has the Rb/Sr ratio values of 32.08–111.48 (avg. 46.01), and the relatively high A/CNK (1.05–1.19) and K_2O/Na_2O (1.01–1.94) ratio values; meanwhile contains muscovite and garnet which are the diagnostic minerals of S-type granite. In conclusion, the Shuitou pluton should be classified as S-type granite.

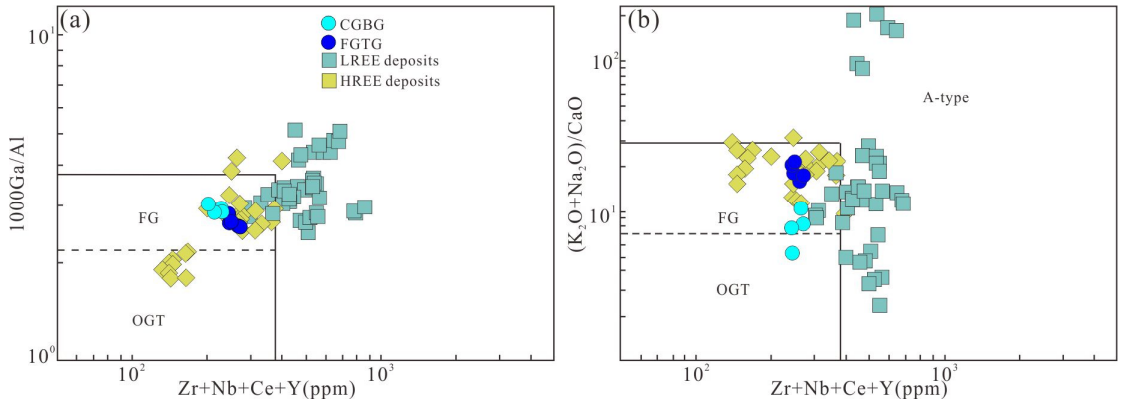

Figure 12. (a) Zr+Nb+Ce+Y vs. 10000Ga/Al, and (b) Zr+Nb+Ce+Y vs. (K_2O+Na_2O)/CaO (Whalen et al., 1987) diagrams for the Shuitou pluton. The data are from reference [18,62].

5.2. Magma Source

Studies have shown that S-type granite magmas originate from metasetamorphic rocks [63]. The source rock compositions can be determined through the CaO/Na_2O ratio. The granite formed from the partial melting of metapelites has the CaO/Na_2O ratio values less than 0.3, and the granite formed from the partial melting of metagraywackes has the values greater than 0.3[64]. The coarse-grained biotite syenogranite in the Shuitou pluton has the CaO/Na_2O values of 0.26–0.56 (avg. 0.38), indicating metagraywackes in its source region, whereas the fine-grained two-mica monzogranite in the Shuitou pluton has the CaO/Na_2O values of 0.10–0.5 (avg. 0.12), indicating metapelites in its source region. These results are basically consistent with the results from the identification diagram of granite source region (Figure 13a). Trace elements are important indicators to distinguish the evolution of granite source regions [65]. The Shuitou pluton has the Nb/Ta ratios of 2.72–9.54 (avg. 5.82), much lower than those of the chondrites (19.9) and the continental crust (13.4)[66] , and has the Zr/Hf ratios of 7.12–26.11 (avg. 16.86), also much lower than those of the chondrites (34.3) and the continental crust (36.7). These indicate that the Shuiton pluton has undergone a highly fractionated rock evolution process, consistent with Figure 12. The value of $Mg^{\#}$ can be used to determine whether the mantle-source material mixing occurred in the source region [67]. The values of $Mg^{\#}$ in the rocks being 2–28 (<40) indicate that that no mantle materials are mixed in the source region. In the samples from the Shuitou pluton, both the zircon Lu–Hf and the monazite Sm–Nd data indicate that granites originate from the anatectic melting or re-melting of ancient crust [68]. Therefore, it is concluded that the source rocks of the Shuitou pluton is the crustal metasedimentary rocks.

 doi:10.20944/preprints202502.2260.v1

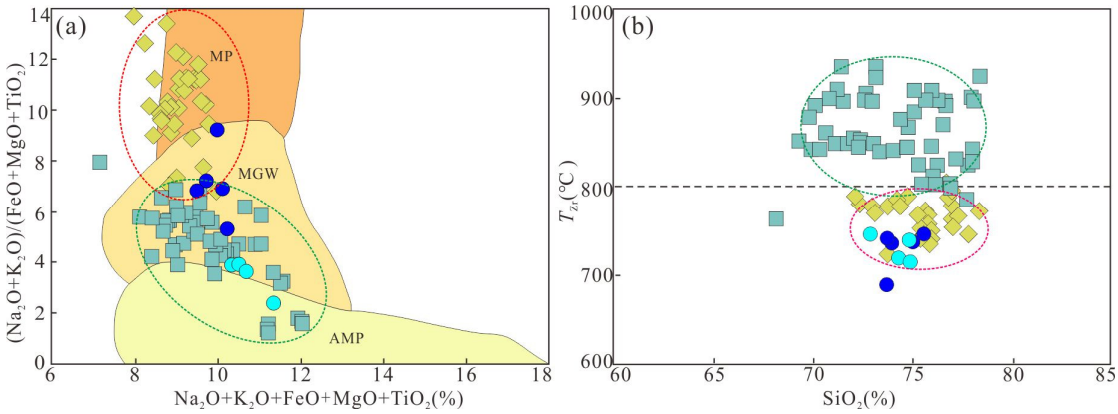

Figure 13. (a) $Na_2O+K_2O+FeO+MgO+TiO_2$ vs. $(Na_2O+K_2O)/(FeO+MgO+TiO_2)$ [69], and (b) Zr vs. T_{Zr} diagrams for the Shuitou pluton. MP = Metapelites; MGW = Metagraywackes; AMP = Amphibolite. The data sources are same as Figure 12. T_{Zr}(°C) is calculated after Watson and Harrison (1983)[70].

5.3. Geodynamic Setting

The Yanshanian tectonic setting in South China has been receiving focused attention from scholars, and various viewpoints have been put forward including the reverse thrusting and overturning [71,72], the continent extending and rifting [73,74] the mantle plume rising [75,77], the multi-phase subducting and retreating model [78,79], and the back-arc extension setting [74,80,81]. The current mainstream viewpoint is that the subduction action of the Paleo-Pacific Plate is the fundamental dynamic mechanism for the formation of the Yanshanian granitic rocks, i.e., the volcanic rocks [22],[26],82[86], but there are still controversies about the precise subduction process. For example, Li et al. (2007)[82] proposed that the Paleo-Pacific Plate initially subducted as flat plate, followed by plate fracturing, delaminating and retreating, Zhou et al. (2006)[22]pointed out that the Yanshanian magmatic rocks became gradually younger from inland to coastal areas, and established a model combining lithosphere subducting and the basaltic magma intruding upward to the lower crust, and proposed that the subduction angle of the slab increased gradually. The third stage (140–125Ma) of magmatic activities in eastern South China occurred in the extensional tectonic setting [74,87,88], and the extensively exposed A-type granites and bimodal volcanic rocks can fully demonstrate that South China was in an back-arc extensional setting during this period.

The samples all fall into the post-collisional tectonic setting in Y vs. Nb diagram (Figure 14a) and (Y+Nb) vs. Rb diagram (Figure 14b), consistent with the tectonic setting of most Late Jurassic granites in South China [82,89]. The subduction angle of the Paleo-Pacific Plate gradually increased from the Jurassic to the Cretaceous period, and the back-arc extending caused by the subduction of the Paleo-Pacific Plate from the NNW or NW trending to the inland at 150 Ma became continuously enhanced, and formed a large amount of Late Jurassic-Early Cretaceous magmatic belts, with the magmatites becoming younger and younger from the inland of South China to the southeast coast [22]. The retreading of the subducting slab caused the thinning of both the crust and the lithospheric mantle, and the fluids released by the upwelling asthenosphere induced the mantle melting and produced the ferromagnesian magma which intruded upward into the Precambrian basement and formed the granitic magma.

 doi:10.20944/preprints202502.2260.v1

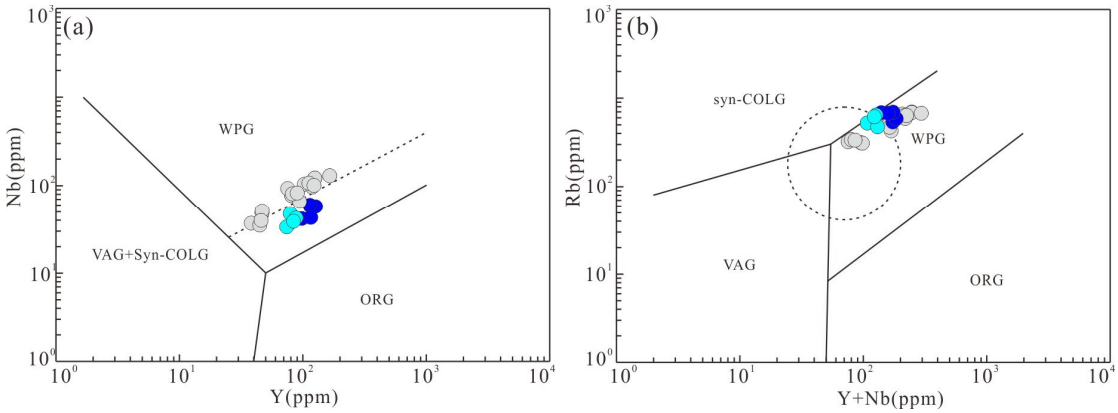

Figure 14. (a) Nb vs. Y, and (b) Y+Nb vs. Rb diagrams for the Shuitou pluton (after Pearce et al., 1984[90]).The data sources are same as Figure 7.

5.4. Implications for REE Enrichment

The ΣREE values of the coarse-grained biotite syenogranite (CGBG) and the fine-grained two-mica monzogranite (FGTG) samples from the Shuitou pluton are 166–236ppm, greater than the REE threshold (150ppm) of the ion-adsorption rare-earth depostit parent rocks in South China. Therefore, these granites can form ion-adsorption rare earth deposits after undergoing natural weathering.

Petrogenetic type is not the key factor controlling the REE content in the granite, and I-type, S-type and A-type granites can all form ion-adsorption rare earth deposits after undergoing natural weathering [18]. Statistical analyses of the geochemical characteristics of the light and heavy rare earth ore-forming parent rocks in South China indicate that the light rare earth ore-forming parent rocks are dominantly the A-type granite (Figure 12), with greater A/CNK ratios and higher formation temperature, and mainly originating from the partial melting of the metagraywackes; whereas the heavy rare earth ore-forming parent rocks are dominantly the highly fractionated I-type or S-type granite, with lower formation temperature, and mainly originating from the partial melting of the metapelites (Figure 13a). The formation of the ion-adsorption rare earth deposits in South China is influenced by the factors such as climate, topography, hydrodynamics and microorganisms, and besides it also relates to the special tectonic setting [93]. The formation age of the ion-adsorption rare-earth deposit parent rocks in South China is mainly 150–190 Ma, with the Mesozoic granite formed in an extensional tectonic setting. The high temperature environment generated by the mantle fluids is conducive to the formation of A-type and S-type granites (Figure 15), and can prompt the partial melting of REE-enriched accessory minerals, which is confirmed by the positive correlation between zirconium saturation temperature and REE content [93]. The subduction of the Mesozoic slab in South China caused the decomposition of some minerals such as the polysilicic muscovite and released a large amount of F-enriched fluids. The higher content of F can increase the solubility of REEs in the molten mass, resulting in a higher REE content in the Shuitou pluton. Furthermore, the REE-enriched minerals such as the garnet, titanite, bastnaesite and allanite in the Shuitou pluton also provide the material basis for the formation of the ion-adsorption REE deposit.

 doi:10.20944/preprints202502.2260.v1

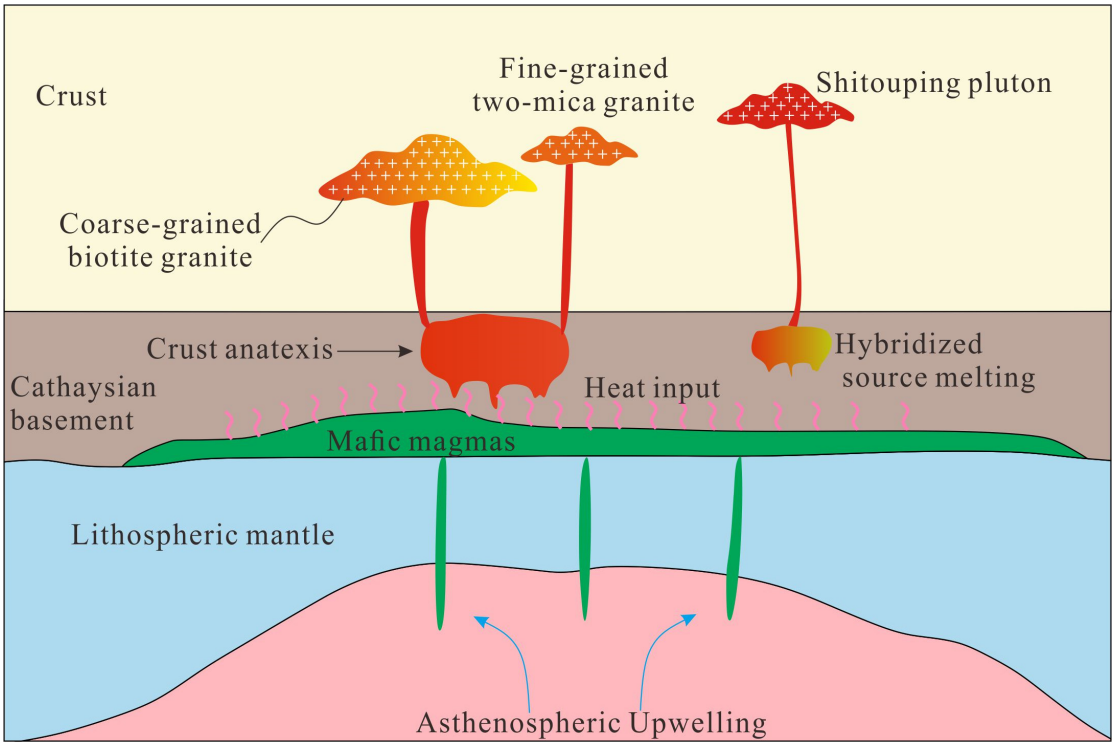

Figure 15. Cartoon showing the generation of Shuitou pluton.

6. Conclusions

(1) The Shuitou pluton is formed at about 150 Ma, contains Al-enriched minerals such as muscovite and garnet, has a high A/CNK value, and belongs to S-type granite.

(2) The $\varepsilon_{Hf}(t)$ values of zircon in the coarse-grained biotite syenogranite (CGBG) are –10.04 to –6.78, and the $\varepsilon_{Hf}(t)$ values of monazite in the fine-grained two-mica monzogranite (FGTG) are –9.3 to –8.2, indicating that the Shuitou pluton originates from the partial melting of lower crustal sedimentary rocks.

(3) The extensional tectonic setting is conducive to the initial enrichment of the rare earth elements in the granite, and the higher content of F increases the solubility of the REEs in the molten mass. Furthermore, the REE-enriched minerals such as the garnet, titanite, bastnaesite and allanite in the Shuitou pluton also provide the material basis for the formation of the ion-adsorption REE deposit.

Supplementary Materials: The following supporting information can be downloaded at the website of this paper posted on Preprints.org.

Data Availability: All data generated or analyzed during this study are included in this article.

Declaration of Competing Interest: The authors declare that they have no known competing financial interests or personal relationships that could have appeared to influence the work reported in this paper.

Funding Projects: The author(s) declare that financial support was received for the research, authorship, and/or publication of this article. The research is supported by the Geological Exploration Project of Jiangxi province Finance (No.20220014), Science and Technology Innovation Project of Department of Natural Resources of Jiangxi province (No.ZRKJ20232411; No.ZRKJ20232526) and Key Laboratory of Ionic Rare Earth Resources and Environment, Ministry of Natural Resources of the People's Republic of China (NO.2022IRERE103; 2023IRERE106).

 doi:10.20944/preprints202502.2260.v1

References

1. Zhou, J.; Wang, X.Q.; Nie, L.S.; McKinley, J.M.; Liu, H.L.; Zhang, B.M.; Han Z.X. Geochemical background and dispersion pattern of the world's largest REE deposit of Bayan Obo, China. *J. Geochem. Explor.* 2020, 215, 106545. doi.10.1016/j.gexplo.2020.106545
2. Kynicky, J.; Smith, M.P.; Xu, C. Diversity of rare earth deposits: The key example of China. *Elements* 2012, 8(05), 361–367. doi.10.2113/gselements.8.5.361
3. Jowitt, S.M; Wong, V.N.L.; Wilson, S.; Gore, O. Critical metals in the critical zone: controls, resources and future prospectivity of regolith-hosted rare earth elements. *Aust. J. Earth Sci.* 2017, 64, 1045–1054. doi.10.1080/08120099.2017.1380701
4. Gulley, A.L.; Nassar, N.T.; Xun. S.A. China, the United States, and competition for resources that enable emerging technologies. *Proc. Natl. Acad. Sci. USA.* 2018, 115, 4111–4115. doi.10.1073/pnas.1717152115
5. Fu, W.; Li. X.T.; Feng, Y.Y.; Feng, M.; Peng, Z.; Yu, H.X.; Lin, H.R. Chemical weathering of S-type granite and formation of rare earth element (REE)-rich regolith in South China: Critical control of lithology. *Chem. Geol.* 2019, 520(03), 33–51. doi.10.1016/j.oregeorev.2019.103120
6. Bao, Z.W.; Zhao, Z.H. Geochemistry of mineralization with exchangeable REY in the weathering crusts of granitic rocks in South China. *Ore Geol. Rev.* 2008, 33(03), 519–535. doi.10.1016/j.oregeorev.2007.03.005
7. Li, M.Y.H.; Zhou, M.F. The role of clay minerals in formation of the regolith-hosted heavy rare earth element deposits. *Am. Mineral.* 2020, 105, 92–108. doi.10.2138/am-2020-7061
8. Li, X.R.; Liang, X.L.; He, H.P.; Li, J.T.; Ma, L.Y.; Tan, W.; Zhong, Y.; Zhu, J.X.; Zhou, M.F.; Dong, H.L. Microorganisms accelerate REE mineralization in supergene environments. *Appl. Environ. Microbiol.* 2022, 88(13), e00632-22. doi.10.1128/aem.00632-22
9. Huang, J.; Tan, W.; Liang, X.L.; He, H.P.; Ma, L.Y.; Bao, Z.W.; Zhu, J.X. REE fractionation controlled by REE speciation during formation of the Renju regolith-hosted REE deposits in Guangdong Province, South China. *Ore Geol. Rev.* 2021, 134, 104172. doi.10.1016/j.oregeorev.2021.104172
10. Li, M.Y.H.; Zhao, W.W.; Zhou, M.F. Nature of Parent Rocks, Mineralization Styles and Ore Genesis of Regolith-Hosted REE Deposits in South China: an Integrated Genetic Model. *J. Asian Earth Sci.* 2017, 148, 65–95. doi.10.1016/j.jseaes.2017.08.004
11. Xu, C.; Kynický,J.; Smith, M.P.; Kopriva, A.; Brtnický, M.; Urubek, T.; Song, W.L. Origin of heavy rare earth mineralization in South China. *Nat. Commun.* 2017, 8(01), 1–7. doi.10.1038/ncomms14598
12. Huang, D.H.; Wu, C.Y.; Han, J.Z. REE geochemistry and mineralization characteristics of the Zudong and Guanxi granites, Jiangxi Province. *Acta Geol. Sin.* 1989, 2, 139–157. doi.10.1111/j.1755-6724.1989.mp2002004.x
13. Ishihara, S.; Hua, R.M.; Hoshino, M.; Murakami, H. REE abundance and REE minerals in granitic rocks in the Nanling range, Jiangxi Province, southern China, and generation of the REE-rich weathered crust deposits. *Resour. Geol.* 2008, 58(04), 355–372. doi.10.1111/j.1751-3928.2008.00070.x
14. Sanematsu, K.; Watanabe, Y. Characteristics and genesis of ion adsorption-type rare earth element deposits. *Reviews in Economic Geology*. 2016, 18, 55–79. doi.10.5382/Rev.18.03
15. Zhao, Z.; Wang, D.H.; Bagas, L.; Chen, Z.Y. Geochemical and REE mineralogical characteristics of the Zhaibei Granite in Jiangxi Province, southern China, and a model for the genesis of ion-adsorption REE deposits. *Ore Geol. Rev.* 2022, 140, 104579. doi.10.1016/j.oregeorev.2021.104579
16. Zhao, X.; Li, N.B.; Huizenga, J.M.; Zhang, Q.B.; Yang, Y.Y.; Yan, S.; Yang, W.B.; Niu, H.C. Granitic magma evolution to magmatic-hydrothermal processes vital to the generation of HREEs ion-adsorption deposits: Constraints from zircon texture, U–Pb geochronology, and geochemistry. *Ore Geol. Rev.* 2022, 146(03), 104931. doi.10.1016/j.oregeorev.2022.104931
17. Gong, L.X.; Wang, X.G.; Zhang, D.F.; Zhong, W.; Cao, M.X. Zircon as a Monitoring Tool for the Magmatic-Hydrothermal Process in the Granitic Bedrock of Shitouping Ion-Adsorption Heavy Rare Earth Element Deposit, South China. *Minerals*. 2023, 13, 1402. doi.10.3390/min13111402
18. Cao, M.X.; Wang, X.G.; Zhang, D.F.; Zhang, Y.W.; Gong, L.X.; Zhong, W. Petrogenesis and REE mineralogical characteristics of Shitouping granites in southern Jiangxi Province: Implication for HREE mineralization in South China. *Ore Geol. Rev.* 2024, 168, 106011. doi.10.1016/j.oregeorev.2024.106011

19. He, C.; Xu, C.; Zhao, Z.; Kynicky, J.; Song, W.L.; Wang, L.Z. Petrogenesis and mineralization of REE-rich granites in Qingxi and Guanxi, Nanling region, South China. *Ore Geol. Rev.* 2017, 81, 309–325. doi.10.1016/j.oregeorev.2016.10.021
20. Fan, C.X.; Xu, C.; Shi, A.G.; Smith, M.P.; Kynicky, J.; Wei, C.W. Origin of heavy rare earth elements in highly fractionated peraluminous granites. *Geochim. Cosmochim. Acta.* 2023, 343, 371–383. doi.10.1016/j.gca.2022.12.019
21. Hua, R.M.; Zhang, W.L.; Gu, S.Y.; Chen, P.R. Comparison between REE granite and W-Sn granite in the Nanling region, South China and their mineralizations. *Acta Petrol. Sin.* 2007, 23(10), 2321–2328. doi:10.3969/j.issn.1000-0569.2007.10.001
22. Zhou, X.M.; Sun, T.; Shen, W.Z.; Shu, L.S.; Niu, Y.L. Petrogenesis of Mesozoic granitoids and volcanic rocks in South China: A response to tectonic evolution. *Episodes* 2006, 29(01), 26–33. doi.10.18814/epiiugs/2006/v29i1/004
23. Li, Z.X.; Li, X.H. Formation of the 1300-km-wide intracontinental orogen and postorogenic magmatic province in Mesozoic South China: a flat-slab subduction model. *Geology* 2007, 35(02), 179–182. doi.10.1130/G23193A.1
24. Fu, W.; Zhao, Q.; Luo, P.; Li, P.Q.; Lu, J.P.; Zhou, H.; Yi, Z.B.; Xu, C. Mineralization diversity of ion-adsorption type REE deposit in southern China and its critical influence by parent rocks. *Acta Geol. Sin.* 2022, 96(11), 3901–3925. doi.10.19762/j.cnki.dizhixuebao.2022233
25. Tao, J.H.; Li, W.X.; Wyman, D.A.; Wang, A.D; Xu, Z.T. Petrogenesis of Triassic Granite from the Jintan Pluton in Central Jiangxi Province, South China: Implication for Uranium Enrichment. *Lithos* 2018, 320-321, 62–74. doi.10.1016/j.lithos.2018.09.003
26. Mao, J.W.; Cheng, Y.B.; Chen, M.H.; Piraino, F. Major types and time-space distribution of Mesozoic ore deposits in South China and their geodynamic settings. *Miner. Deposita* 2013, 48, 267–294. doi.10.1007/s00126-012-0446-z
27. Li, C.Y.; Zhang, H.; Wang, F.Y.; Liu, J.Q.; Sun, Y.L.; Hao, X.L.; Li, Y.L.; Sun, W. The formation of the Dabaoshan porphyry molybdenum deposit induced by slab rollback. *Lithos* 2012, 150, 101–110. doi.10.1016/j.lithos.2012.04.001
28. Jiang, X.Y.; Li, X.H.; Collins, W.J.; Huang, H.Q. U–Pb age and Hf–O isotopes of detrital zircons from Hainan Island: Implications for Mesozoic subduction models. *Lithos* 2015, 239, 60–70. doi.10.1016/j.lithos.2015.10.006
29. Xu, X.S.; Zhao, K.; He, Z.Y.; Liu, L.; Hong, W.T. Cretaceous volcanic-plutonic magmatism in SE China and a genetic model. *Lithos* 2021, 402–403, 105728. doi. 10.1016/j.lithos.2020.105728
30. Li, M.Y.H.; Zhou, M.F.; Williams-Jones, A.E. The genesis of regolith-hosted heavy rare earth element deposits: Insights from the world-class Zudong deposit in Jiangxi Province, South China. *Econ. Geol.* 2019, 114(03), 541–568. doi.10.5382/econgeo.4642
31. Yang, S.W.; Lou, F.S.; Zhang, F.R.; Ding, P.X.; Cao, Y.B.; Xu, Z.; Sun, C.; Feng, Z. H.; Ling, L.H. Anatexis-ceremonies magmatism activity of the Qishan granitic pluton in Southern Jiangxi: chronological study of zircon U–Pb precise dating. *Acta Geol. Sin.* 2017, 91(04), 864–875. doi.10.3969/j.issn.0001-5717.2017.04.012
32. Zhang, D.F.; Cao, M.X.; Gong, X.; Gong, L.X.; Zhong, W.; Qiu, W.J.; Wang, X.G. Geological characteristics of metallogenic host rock and their genetic significance of Shitouping heavy rare earth deposit in Southern Jiangxi Province. *J. East China Univ. Technol., Nat. Sci.* 2024, 47(04), 338–348.doi.10.3969/j.issn.1674-3504.2024.04.004
33. Cen, T.; Li, X.W.; Tao, J.H., Zhao, X.L., Xing, G.F. Geochronology, geochemistry and zircon Hf isotope for Banshi and Caifang volcanic rocks from southern Jiangxi province and their geological implications. *Geotecton. Metallog.* 2017, 41(05), 933–949. doi.10.16539/j.ddgzyckx.2017.05.010
34. Li, Q.; Zhao, K.D.; Palmer, M.R.; Chen, W.; Jiang, S.Y. Exploring volcanic-intrusive connections and chemical differentiation of high silica magmas in the Early Cretaceous Yanbei caldera complex hosting a giant tin deposit, Southeast China. *Chem. Geol.* 2021, 584, 120501. doi.10.1016/j.chemgeo.2021.120501
35. Sun, T. A new map showing the distribution of granites in South China and its explanatory notes. *Geol. Bull. China.* 2006, 25(3), 332-335. doi.10.3969/j.issn.1671-2552.2006.03.002

36. Liu, Y.S.; Gao, S.; Hu, Z C.; Wang, D.B. Continental and oceanic crust recycling-induced melt-peridotite interactions in the Trans-North China Orogen: U–Pb dating, Hf isotopes and trace elements in zircons of mantle xenoliths. *J. Petrol*. 2010, 51(1/2), 537–571. doi.10.1093/petrology/egp082
37. Ludwig, K.R. User's Manual for Isoplot 3.00-A Geochronological Toolkit for Microsoft Excel. 2003.
38. Blichert-Toft, J.; Albarède, F. The Lu–Hf isotope geochemistry of chondrites and the evolution of the mantle-crust system. *Earth Planet. Sci. Lett*. 1997, 148(1/2), 243–258. doi.10.1016/S0012-821X(97)00040-X
39. Griffin, W.L.; Pearson, N.J.; Belousova, E.; Jackson, S.E.; Achterbergh, E, O'Reilly, S.Y.; Shee, S.R. The Hf isotope composition of cratonic mantle: LAM-MC-ICPMS analysis of zircon megacrysts in kimberlites. *Geochim. Cosmochim. Acta* 2000, 64(01), 133–147. doi.org/10.1016/S0016-7037(99)00343-9
40. Griffin, W.L.; Wang, X.; Jackson, S.E.; Pearson, N.J.; O'Reilly, S.Y.; Xu, X.S.; and Zhou, X.M. Zircon geochemistry and magma mixing, SE China: In-situ analysis of Hf isotopes, Tonglu and Pingtan igneous conplexes. *Lithos* 2002, 61(3/4), 237–269. doi.org/10.1016/S0024-4937(02)00082-8
41. Zhang, W.; Hu, Z.C.; Liu, Y.S. Iso-Compass: New freeware software for isotopic data reduction of LA-MC-ICP-MS. *J. Anal. At. Spectrom*. 2020, 35(06), 1087–1096. doi.10.1039/D0JA00084A
42. Xu, L.; Hu, Z.C.; Zhang, W.; Yang, L.; Liu, Y.S.; Gao, S.; Luo, T.; Hu, S.H. In situ Nd isotope analyses in geological materials with signal enhancement and non-linear mass dependent fractionation reduction using laser ablation MC-ICP-MS. *J. Anal. At. Spectrom*. 2015, 30(01), 232–244. doi.10.1039/C4JA00243A
43. Middlemost, E.A.K. Naming materials in the magma/igneous rock system. *Earth Sci. Rev*. 1994, 37(3/4), 215–224. doi.10.1016/0012-8252(94)90029-9
44. Peccerillo, R.; Taylor, S.R. Geochemistry of eocene calc-alkaline volcanic rocks from the Kastamonu area, Northern Turkey. *Contr. Mineral. Petrol*. 1976, 58, 63–81. doi.10.1007/BF00384745
45. Middlemost, E.A.K. Magmas and magmatic rocks. London: Longman. 1985, 1–266. doi.10.1017/S0016756800026716
46. Maniar, P.D.; Piccoli, P.M. Tectonic discrimination of granitoids. *Geol. Soc. Am. Bull*. 1989, 101(05), 635–643. doi.10.1130/0016-7606(1989)101%3C0635:TDOG%3E2.3.CO;2
47. Frost, B.R.; Barnes, C.G.; Collins, W.J.; Arculus, R.J.; Ellis, D.J.; Frost, C.D. A geochemical classification for granitic rocks. *J. Petrol*. 2001, 42, 2033–2048. doi.10.1093/petrology/42.11.2033
48. Zhang, Q.; Wang, X.; Li, C.D.; Jin, W.J.; Jia, X.Q. A granite classification based on pressures. *Geol. Bull. Geol. Surv. China*. 2006, 25(11), 1274–1278. doi.10.3969/j.issn.1671-2552.2006.11.004
49. Sun, S.S.; McDonough, W.F. Chemical and isotopic systematics of oceanic basalts: implications for mantle composition and processes. *Geol. Soc. Spec. Publ*. 1989, 42 (01), 313–345. doi.10.1144/gsl.sp.1989.042.01.19
50. Wu, F.Y.; Li, X.H.; Zheng, Y.F.; Gao, S. Lu–Hf isotopic systematics and their applications in petrology. *Acta Petrol. Sin*. 2007, 23(02), 185–220. doi.10.3969/j.issn.1000-0569.2007.02.001
51. Amelin, Y.; Lee, D.C.; Halliday, A.N.; Pidgeon, R.T. Nature of the Earth's earliest crust from hafnium isotopes in single detrital zircons. *Nature*. 1999, 399(6733), 252–255. doi.10.1038/20426
52. Vervoort, J.D.; Patchett, P.J.; Blichert-Toft, J.; Albarède, F. Relationships between Lu–Hf and Sm–Nd isotopic systems in the global sedimentary system. *Earth Planet. Sci. Lett*. 1999, 168(1/2), 79–99. doi.10.1016/S0012-821X(99)00047-3
53. Liu, X.; Liang, H.; Wang, Q.; Ma, L.; Yang, J.H.; Guo, H.F.; Xiong, X.L.; Ou, Q.; Zeng, J.P.; Gou, G.N.; Hao, L.L. Early Cretaceous Sn-bearing granite porphyries, A-type granites, and rhyolites in the Mikengshan-Qingxixiang-Yanbei area, South China: Petrogenesis and implications for ore mineralization. *J. Asian Earth Sci*. 2022, 235, 105274. doi.10.1016/j.jseaes.2022.105274
54. Chappell, B.W.; White, A.J.R. Two contrasting granite types. *Pac. Geol*. 1974, 8(02), 172–174. doi.10.1016/j.jseaes.2022.105274
55. White, W.M.; Tapia, M.D.M.; Schilling, J.G. The petrology and geochemistry of the Azores Islands. *Contrib. Mineral. Petrol*. 1979, 69(03), 201–213. doi.10.1007/BF00372322
56. Chappell, B.W. Aluminium saturation in I-and S-type granites and the characterization of fractionated haplogranites. *Lithos* 1999, 46(03), 535–551. doi.10.1016/S0024-4937(98)00086-3
57. Champion, D.C.; Chappell, B.W. Petrogenesis of felsic I-type granites: an example from northern Queensland. *Earth Environ. Sci. Trans. R. Soc. Edinburgh.* 1992, 83(1/2), 115–126. doi.10.1017/S026359330000780X

58. Whalen, J.B.; Currie K.L.; Chappell, B.W. A-type granites: geochemical characteristics, discrimination and petrogenesis. *Contrib. Mineral. Petrol.* 1987, 95, 407–419. doi.10.1007/BF00402202
59. King, P.L.; Chappell, B.W.; Allen, C.M.; White, A.J.R. Are A-type granites the high-temperature felsic granites? Evidence from fractionated granites of the Wangrah Suite. *Aust. J. Earth Sci.* 2001, 48(4), 501–514. doi.10.1046/j.1440-0952.2001.00881.x
60. Loiselle, M.C.; Wones, D.R. Characteristics and origin of anorogenic granites. *Geol. Soc. Am. Bull.* 1979, 11, 468.
61. King, P.L.; White, A.J.R.; Chappell, B.W.; Allen, C.M. Characterization and origin of aluminous A-type granites from the Lachlan fold belt, Southeastern Australia. *J. Petrol.* 1997, 38(03), 371–391. doi.10.1093/petroj/38.3.371
62. Yang, Y.Y; Li, N.B.; Jiang, Y.H; Zhao, X. Geochemical differences of parent rocks for ion-adsorption LREE and HREE deposits: A case study of the Guanxi and Dabu granite plutons. *Geotecton. Metallog.* 2024, 48(02), 232–247. doi/10.16539/j.ddgzyckx.2024.02.004
63. Chappell, B.W.; White, A.J.R.; Wyborne, D. The importance of residual source material (Restite) in granite petrogenesis. *J. Petrol.* 1987, 28(06), 1111–1138. doi.10.1093/petrology/28.6.1111
64. Sylvester, P.J. Post-collisional strongly peraluminous granites. *Lithos* 1998, 45(1/2/3/4), 29–44. doi.10.1016/S0024-4937(98)00024-3
65. Zhao, Z.H.; Zhou, L.D. REE geochemistry of some alkali-rich intrusive rocks in China. *Sci. China Ser. D-Earth Sci.* 1997, 40(02), 145–158. doi:10.1007/BF02878373
66. Taylor, S.R.; Mc Lennan, S.M. The geochemical evolution of the continental crust. *Rev. Geophys.* 1995, 33(02), 241–265. doi.10.1029/95RG00262
67. Rapp, R.P.; Watson, E.B. Dehydration melting of metabasalt at 8-32 kbar: implications for continental growth and crust-mantle Recycling. *J. Petrol.* 1995, 36(04), 891–931. doi.10.1093/petrology/36.4.891
68. Zhu, D.C.; Mo, X.X.; Wang, L.Q.; Zhao, Z.D.; Niu, Y.L.; Zhou, C.Y.; Yang, Y.H. Petrogenesis of highly fractionated I-type granites in the Zayu area of eastern Gangdese, Tibet: constraints from zircon U–Pb geochronology, geochemistry and Sr–Nd–Hf isotopes. *China Ser. D-Earth Sci.* 2009, 52(09), 1223–1239. doi:10.1007/s11430-009-0132-x
69. Patiño Douce, A.E. What do experiments tell us about the relative contributions of crust and mantle to the origin of granitic magmas? *Geol. Soc. Spec. Publ.* 1999, 168(01), 55–75. doi.10.1144/GSL.SP.1999.168.01.05
70. Watson, E.B.; Harrison, T. M. Zircon saturation revisited: temperature and composition effects in a variety of crustal magma types. *Earth Planet. Sci. Lett.* 1983, 64, 295–304. doi.10.1016/0012-821X(83)90211-X
71. Hsü K.J, Sun, S.; Li, J.L.; Chen, H.L.; Pen, H.P.; Sengor, A.M.C. Mesozoic overthrust tectonics in south China. *Geology* 1988, 16(05), 418–421. doi.10.1130/0091-7613(1988)016<0418:MOTISC>2.3.CO;2
72. Walter, T.R.; Troll, V.R.; Cailleau, B.; Belousov, A.; Schmincke, H.U.; Amelung, F.; Bogaard, P.V.D. Rift zone reorganization through flank instability in ocean island volcanoes: an example from Tenerife, Canary Islands. *Bull. Volcanol.* 2005, 67(04), 281–291. doi.10.1007/s00445-004-0352-z
73. Gilder, S.A.; Gill, J.B.; Coe, R.S.; Zhao, X.; Liu, Z.; Wang, G.; Yuan, K.; Liu, W.; Kuang, G.; Wu, H. Isotopic and paleomagnetic constraints on the Mesozoic tectonic evolution of south China. *J. Geophys. Res. : Solid Earth.* 1996, 101(B7): 16137–16154. doi.10.1029/96JB00662
74. Li, X.H. Cretaceous magmatism and lithospheric extension in southeast China. *J. Asian Earth Sci.* 2000, 18(03), 293–305. doi.10.1016/S1367-9120(99)00060-7
75. Mao, J.R.; Tao, K.Y.; Xing, G.F.; Yang, Z.L.; Zhao,Y. Petrological records of the Mesozoic-Cenozoic mantle plume tectonics in epicontinental area of Southeast China. *Acta Geosci. Sin.* 1999, 20(03), 253–258. doi:10.3321/j.issn:1006-3021.1999.03.006
76. Xie, G.Q.; Hu, R.Z.; Zhao, J.H.; Jiang, G.H. Mantle plume and the relationship between it and mesozoic large-scale metallogenesis in Southeastern China: A preliminary discussion. *Geotecton. Metallog.* 2001, 25(02), 179–186. doi.10.3969/j.issn.1001-1552.2001.02.010
77. Deng, J.F.; Mo, X.X.; Zhao, H.L; Wu, Z.X.; Luo, Z.H.; Su, S.G. A new model for the dynamic evolution of Chinese lithosphere: 'continental roots-plume tectonics'. *Earth-Sci. Rev.* 2004, 65(3/4), 223–275. doi.10.1016/j.earscirev.2003.08.001

78. Mao, J.R.; Xu, N,Z.; Hu, Q.; Xing, G.F.; Yang, Z.L. The Mesozoic rock-forming and ore-forming processes and tectonic environment evolution in Shanghang-Datian region, Fujian. *Acta Petrol. Sin*. 2004, 20(02), 285–296. doi:10.3969/j.issn.1000-0569.2004.02.010
79. Li, J.H.; Dong, S.W.; Zhang, Y.Q.; Zhao, G.C.; Johnston, S.T.; Cui, J.J.; Xin, Y.J. New insights into Phanerozoic tectonics of south China: Part 1, polyphase deformation in the Jiuling and Lianyunshan domains of the central Jiangnan Orogen. *J. Geophys. Res*. : *Solid Earth.* 2016, 121(04), 3048–3080. doi.10.1002/2015JB012778
80. Shinjo, R.; Kato, Y. Geochemical constraints on the origin of bimodal magmatism at the Okinawa Trough, an incipient back-arc basin. *Lithos* 2000, 54, 117–137. doi.10.1016/S0024-4937(00)00034-7
81. Brewer, T.S.; Åhäll, K.I.; Menuge, J.F.; Storey, C.; Parrish, R. Mesoproterozoic bimodal volcanism in SW Norway, evidence for recurring pre-Sveconorwegian continental margin tectonism. *Precambrian Res*. 2004, 134, 249–273. doi.10.1016/j.precamres.2004.06.003
82. Li, X.H.; Li, Z.X.; Li, W.X.; Liu, Y.; Yuan, C.; Wei, G.J.; Qi, C.S. U–Pb zircon, geochemical and Sr–Nd–Hf isotopic constraints on age and origin of Jurassic I- and A- type granites from central Guangdong, SE China: A major igneous event in response to foundering of a subducted flat-slab? *Lithos* 2007, 96, 186–204. doi.10.1016/j.lithos.2006.09.018
83. Mao, J.W.; Xie, G.Q.; Guo, C.L.; Chen, Y.C. Large-scale tungsten-tin mineralization in the Nanling region, South China: Metallogenic ages and corresponding geodynamic processes. Sinica, *Acta Petrol*. 2007, 23(10), 2329–2338. doi.10.3969/j.issn.1000-0569.2007.10.002
84. Chen, C.H.; Lee, C.Y.; Shinjo, R. Was there Jurassic paleo-Pacific subduction in South China?: Constraints from $^{40}Ar/^{39}Ar$ dating, elemental and Sr-Nd-Pb isotopic geochemistry of the Mesozoic basalts. *Lithos* 2008, 106(1/2), 83–92. doi.10.1016/j.lithos.2008.06.009
85. Li, Y.; Ma, C;Q.; Xing, G.F.; Zhou, H;W. The Early Cretaceous evolution of SE China; Insights from the Changle-Nan'ao Metamorphic Belt. *Lithos* 2015, 230, 94–104. doi.10.1016/j.lithos.2015.05.014
86. Zhang, Z.Y.; Hou, Z.Q.; Lü, Q.T.; Zhang, X.W.; Pan, X.F.; Fan, X.K.; Zhang, Y.Q.; Wang, C.G.; Lü, Y.J. Crustal architectural controls on critical metal ore systems in South China based on Hf isotopic mapping. *Geology* 2023, 51(08), 738–742. doi.org/10.1130/G51203.1
87. Wang, Y.J, Fan, W.M.; Cawood, P.A.; Li, S.Z. Sr–Nd–Pb isotopic constraints on multiple mantle domains for Mesozoic mafic rocks beneath the South China Block hinterland. *Lithos* 2008, 106(3/4), 297–308. doi.10.1016/j.lithos.2008.07.019
88. Zhou, J.; Jiang, Y.H.; Xing, G.F.; Zeng, Y.; Ge, W.Y. Geochronology and petrogenesis of Cretaceous A-type granites from the NE Jiangnan Orogen, SE China. *Int. Geol. Rev.* 2013, 55(11), 1359–1383. doi.10.1080/00206814.2013.774199.
89. He, Z.Y.; Xu, X.S. Petrogenesis of the Late Yanshanian mantle-derived intrusions in southeastern China; Response to geodynamics of paleo-Pacific plate subduction. *Chem. Geol*. 2012, 328, 208–221. doi.10.1016/j.chemgeo.2011.09.014
90. Pearce, J.A.; Harris, N.B.W.; and Tindle, A.G. Trace element discrimination diagrams for the tectonic interpretation of granitic rocks. *J. Petrol*. 1984, 25(04), 956–983. doi.10.1093/petrology/25.4.956
91. Fu, W.; Luo, P.; Hu, Z.Y.; Feng, Y.Y.; Peng, Z.; Liu, L.; Yang, J.B.; Feng,M.; Yu, H.X.; Zhou, Y.Z. Enrichment of ion-exchangeable rare earth elements by felsic volcanic rock weathering in South China: Genetic mechanism and formation preference. *Ore Geol. Rev*. 2019, 103120. doi.10.1016/j.chemgeo.2019.05.006
92. Zhang, D.F.; Lv, T.T.; Wang, X.G.; Cao, M.X.; Chen, X.Q.; Zhang, Y.W.; Gong, L.X. Petrogenesis of REE-rich two-mica granite from the Indosinian Xiekeng pluton in South China Block with implications for REE metallogenesis. *Front. Earth Sci*. 2025. doi.org/10.3389/feart.2024.149359
93. Zhao, X.; Li, N.B.; Huizenga, J.M.; Yan, S.; Yang, Y.Y.; Niu, H.C. Rare earth element enrichment in the ion-adsorption deposits associated granites at Mesozoic extensional tectonic setting in South China. *Ore Geol. Rev*. 2021, 137, 104317. doi.10.1016/j.oregeorev.2021.104317